Finite-size scaling effect on Néel temperature of antiferromagnetic Cr_2O_3-(0001) films in an exchange-coupled heterostructure

Satya Prakash Pati,* Muftah Al-Mahdawi,† Shujun Ye,
Yohei Shiokawa, Tomohiro Nozaki, and Masashi Sahashi
Department of Electronic Engineering,
Tohoku University, Sendai 980-8579, Japan

(Dated: January 5, 2017)

arXiv:1608.04531v2 [cond-mat.mes-hall] 4 Jan 2017

Abstract

The scaling of antiferromagnetic ordering temperature of corundum-type chromia films have been investigated. Néel temperature T_N was determined from the effect of perpendicular exchange-bias on the magnetization of a weakly-coupled adjacent ferromagnet. For a thick-film case, the validity of detection is confirmed by a susceptibility measurement. Detection of T_N was possible down to 1-nm-thin chromia films. The scaling of ordering temperature with thickness was studied using different buffering materials, and compared with Monte-Carlo simulations. The spin-correlation length and the corresponding critical exponent were estimated, and they were consistent between experimental and simulation results. The spin-correlation length is an order of magnitude less than cubic antiferromagnets. We propose that the difference is from the change of number of exchange-coupling links in the two crystal systems.

I. INTRODUCTION

In correlated systems, the physical properties during a phase transition are altered in reduced dimensions comparable in size to a certain characteristic correlation length[1]. Thin films, nano-wires, and nano-particles are suitable to study confinement in one or more dimensions. The advances in fabrication of epitaxial films made them the most relevant in many technological applications. In the weakly-correlated superconductors, the correlation length is in order of tens to hundreds of nanometers[2], thus the finite-size scaling (FSS) effects of reducing the phase-transition temperature are observed in rather thick films[3]. In ferroelectrics, FSS effects appear on thinner films of a few tens of nanometers[4]. However, in strongly-correlated systems such as ferromagnets (FMs) and antiferromagnets (AFMs) the correlation length is much shorter[5]. Spin-correlation length measurements based on FSS in simple-cubic, body-centered cubic, and close-packed lattices were readily reported[5]. The corresponding critical exponent estimations in these common lattices were also widely studied[6–10]. However, studies on corundum-type magnetic materials are only a few[11]. In the report by He *et al.*[11], the blocking temperature of exchange-bias data were considered rather than Néel temperatures. Monte-Carlo (MC) simulation studies of corundum-type Cr_2O_3 were reported before[12,13]. However, estimations of spin-correlation length and the corresponding critical exponent ν were not investigated.

The research on Cr_2O_3 has gained a renewed interest for exploration of voltage-controlled magnetic states near to room temperature[14–19]. These findings opened a pathway to utilize chromia in voltage-controlled spintronic devices[14,20] including hard-disk-drive media[21,22]. For applications requiring a low switching voltage, it is required to fabricate high-quality continuous ultrathin chromia films while retaining the magnetic properties. However, the thermal stability and the operating temperature of the device may decrease by using ultrathin films, due to the FSS effect on Néel temperature and the low AFM anisotropy. Recently, there were some efforts to enhance the thermal stability of chromia. The effect of lattice strain induced by lattice mismatch on T_N was demonstrated theoretically[23], as well as experimentally[24]. Also, an enhancement of T_N by boron doping in the anion sites of Cr_2O_3 was also predicted theoretically[25], and confirmed experimentally[26]. Another approach is the spin-correlation effect, where the length of spin correlation increases more than twice the bulk value when Cr_2O_3 is laminated with Fe_2O_3 with an oxygen-divided interface[13]. It was reported that a

Table I. The inplane lattice constants of a 20-nm Cr_2O_3 layer over different buffer layers[24], and for the simulated crystal. Also, the deduced values from section IV of Néel temperature T_N^∞, correlation length ξ_0, and shift exponent λ are included.

Buffer layer	a [Å]	T_N^∞ [K]	ξ_0 [nm]	λ
α-Fe_2O_3[a]	5.04[b]	266		
α-Ir-Fe_2O_3	5.02[b]	281	0.57(6)	1.34(7)
Pt[a]	4.98	297		
Simulation 1	4.95	300	0.20(2)	1.37(2)
Simulation 2	4.95	306	0.24(2)	1.26(1)

[a] From Ref. 24.

[b] Assuming that Cr_2O_3 films has a pseudomorphic growth over Fe_2O_3[24,34].

strong exchange-coupling at the interface between two AFMs having different T_N's and AFM anisotropies can enhance either one when the thickness reaches the spin-correlation length, as exemplified in a CoO/NiO bilayer system[27]. However, an experimental determination of the spin-correlation length in Cr_2O_3 has not been reported.

FSS observations on AFMs are a challenge because of the diminishing stray magnetization. The shift in the Néel temperature T_N in ultra-thin AFM films was detected by *ac* susceptibility[28], neutron diffraction[29], specific heat[30,31], x-ray magnetic linear dichroism[32], and spin-current absorption[33]. In this report we demonstrate a simpler method to detect T_N in ultrathin AFMs. By detecting the change of the equilibration angle of the magnetization of an adjacent FM layer, the onset of AFM ordering and T_N can be inferred. After introducing this detection method in section III, we used it to study the shift in T_N of Cr_2O_3 films with thicknesses down to 1 nm in section IV. Additionally, we compared the experimental results with MC simulations.

II. EXPERIMENTAL DETAILS

Heterostructures of Cr_2O_3 (t_{Cr2O3})/Ru (t_{Ru})/Co (1)/Pt (5) were grown over different buffer layers on c-Al_2O_3 substrates. The numbers in parentheses represent thicknesses in nanometer. The buffer layers were Pt (25), α-Fe_2O_3 (20) , and Ir-doped α-Fe_2O_3 (20). The

lattice mismatch with the different buffers was used to control the inplane lattice strain in Cr_2O_3 and hence T_N[23,24]. The buffers had different spin structures, namely non-magnetic for Pt, an in-plane spin orientation for Fe_2O_3[35], and an out-of-plane spin orientation for Ir-Fe_2O_3[35,36]. It was predicted that Cr_2O_3 would have an increased spin correlation length at the interface in the bilayer of Fe_2O_3/Cr_2O_3[37]. Therefore, the investigation of correlation length over buffers with different magnetic structure is needed to explore such effects. The oxide layers were deposited by reactive radio-frequency magnetron sputtering in a mixed atmosphere of argon and oxygen from metal Cr, Fe, and $Ir_{0.1}$-$Fe_{99.9}$ targets. The (Ar, O_2) gas flow in sccm was fixed at (8.0, 2.0) for both of Fe_2O_3 and Ir-Fe_2O_3 growth, and (9.0, 0.85) during Cr_2O_3 growth. All of the buffer layers and Cr_2O_3 layers were grown at 773 K. The other metal layers were grown at 423 K. All of the metal layers were deposited by direct-current sputtering. Deposition rates were determined from the rate calibration and for Pt buffer, Fe_2O_3, Cr_2O_3, Ru, and Co they were 5.45, 0.17, 0.26, 1.44, and 2.86 nm/min within 3% error, respectively.

The conditions for epitaxial growth were chosen to minimize the surface roughness of each layer. In the Fe_2O_3 and Ir-Fe_2O_3 buffers case as an example, atomic-force microscopy showed a roughness average R_a of less than 0.1 nm for both of the buffers and the respectively grown Cr_2O_3 layer. The surface-height histogram of a 1.5-nm Cr_2O_3 layer deposited over an Ir-Fe_2O_3 buffer is shown in Fig. 1, with the surface topography in the inset. The surface is flat with $R_a = 0.09$ nm. We assume that the thickness follows a log-normal distribution of the following form:

$$P_T(t, t_n, s) = \frac{1}{t_{\mathrm{Cr2O3}} s\sqrt{2\pi}} \exp\left(\frac{\ln(t_{\mathrm{Cr2O3}}/t_n)}{\sqrt{2}s}\right)^2, \quad (1)$$

where t_{Cr2O3} is the local thickness, t_n is the median thickness, and s is the shape parameter. A fitting around the average thickness $\langle t_{\mathrm{Cr2O3}}\rangle$ gave $s = 0.036$. The previous assumption of using Eq. 1 to describe the film thickness is solely based on the experimental observation. Eq. 1 is used in section IV to estimate the error introduced by ignoring roughness.

Analysis by X-ray diffraction[24,38] and transmission-electron microscopy[38] indicated the epitaxial growth, the flat sharp interfaces, and the control of lattice strain in the Cr_2O_3 layer over different buffers. The detailed structural studies are presented elsewhere[24,38]. Table I summarizes the inplane lattice parameters of a 20-nm Cr_2O_3 layer over the different buffers, in addition to the lattice parameters used for the simulation mentioned afterwards. The

characterization of magnetic properties was done by a commercial magnetometer based on a superconducting quantum interference device. The magnetometer was set up to measure the out-of-plane component of magnetization, and the magnetic field was applied in the out-of-plane direction. Additionally, we compared experimental results with Monte-Carlo simulations conducted using VAMPIRE atomistic simulation package[39], with a Heisenberg's spin-Hamiltonian formalism.

III. NÉEL TEMPERATURE DETECTION

In our previous report[24], we established a detection technique of T_N, where a change of the magnetization in a low-field magnetization-temperature M-T curve coincides with the enhancement of Co coercivity due to exchange coupling with AFM spins. To detect T_N in ultra-thin Cr_2O_3 films ($\ll$10 nm), we optimized the anisotropy of the exchange-coupled FM layer to compensate the demagnetization field. The ordering of AFM spins at T_N becomes amplified by a tilt in FM magnetization direction from in-plane to out-of-plane at a low applied magnetic field (Fig. 2(a)). A macrospin model of the total energy per unit-area of Co magnetization, composed of demagnetization, total interfacial anisotropy, Zeeman, and exchange coupling energies can be written as follows:

$$\begin{aligned} W_{\mathrm{Co}} &= \left(2\pi M_s^2 t_{\mathrm{Co}} - J_i\right)\cos^2\theta - \left(HM_s t_{\mathrm{Co}} + J_K\right)\cos\theta \\ &\equiv K_{\mathrm{eff}}\cos^2\theta - K_H\cos\theta, \end{aligned} \tag{2}$$

where W_{Co}, θ, t_{Co}, M_s, J_i, J_K are the total areal energy density, the magnetization angle from perpendicular direction, Co thickness, Co saturation magnetization, interfacial anisotropy energy density of the top and bottom interfaces, and exchange coupling energy with Cr_2O_3, respectively. The effective uniaxial and unidirectional anisotropies are represented by K_{eff} and K_H, respectively. A positive (negative) K_{eff} corresponds to an inplane (out-of-plane) easy direction of Co's magnetization. The exchange coupling energy J_K is considered as an effective value representing the average exchange coupling energy through Cr_2O_3/Co interface, which is determined experimentally. Such a simplified model can be used due to the simple collinear alignment of Cr_2O_3 and Co spins, and the dominance of uncompensated surface spins at Cr_2O_3 surface[40]. The normalized perpendicular component of Co magneti-

zation m_z is found from the equilibration angle θ_0 at which the energy is minimized with a stable solution. The relevant solution that has a varying m_z is:

$$m_z = \cos\theta_0 = \frac{K_H}{2K_{\text{eff}}}, \text{where} \left|\frac{K_H}{2K_{\text{eff}}}\right| \leq 1. \quad (3)$$

The term with the strongest temperature-dependence is J_K, which is proportional to the average order parameter of Cr_2O_3. The change of Co saturation magnetization in the temperature range of measurement is negligible. Therefore, the temperature dependence of m_z at a fixed low field $M_r(T)$ and the accompanying change of slope dM_r/dT are related to the ordering of Cr_2O_3 spins at T_N. In order to obtain a large change of equilibrium angle from in-plane above T_N to out-of-plane tilting below T_N, K_{eff} should be $0 < K_{\text{eff}} \lessapprox J_K/2$.

To tune the interfacial anisotropy and the exchange-coupling energies, we used a Ru-metal spacer. We found that Co has an inplane interface anisotropy with Ru, which gives another free parameter for a fine control of Co total anisotropy. In this report, we optimized the thickness of Ru spacer to allow for the detection of T_N down to $t_{\text{Cr2O3}} = 1$ nm. We varied the thickness of Ru t_{Ru} in the stack: Pt (25)/Cr_2O_3 (20)/Ru (t_{Ru})/Co (1)/Pt (5). Figure 2(b) shows the effect of Ru insertion on decreasing the total exchange-coupling energy J_K between Co and Cr_2O_3. For a weak FM/AFM coupling compared to AFM anisotropy, J_K manifests as an exchange-bias field H_{eb}. In the strong coupling case, an increase of FM coercivity ΔH_C over a base value is observed. Thus, J_K was determined from $(H_{\text{eb}} + \Delta H_C)/(M_s t_{\text{Co}})$[24], where the experimental values of $M_s t_{\text{Co}}$ were used[38]. For $t_{\text{Ru}} < 1$ nm, high squareness remained above and below T_N of ≈290 K, and the change of M_r was small (Fig. 2(c)). At intermediate thicknesses of 1.25–1.5 nm, a large change of M_r above and below T_N was found. At more than 1.8 nm of Ru, the exchange coupling was diminished, and detection of T_N was not feasible. Examples of magnetization hysteresis loops at strong and intermediate couplings are shown in Fig. 2(d). We fixed t_{Ru} at 1.25 nm for all subsequent experiments. At this thickness the optimized values of J_K and K_{eff} were obtained at 0.10–0.12 and +0.05 erg/cm^2, respectively. Hence, the condition of $0 < K_{\text{eff}} \lessapprox J_K/2$ is fulfilled.

To confirm that the detected transition temperature is same as T_N, we compared the low-field and high-field M-T dependencies with a rather thick Cr_2O_3 layer. The film structure was Pt (25)/Cr_2O_3 (1000)/Ru (1.25)/Co (1)/Pt (5). The total measured magnetization is composed of Co's magnetization, Cr_2O_3 antiferromangetic susceptibility response χH, and diamgnetic and paramagnetic responses of the substrate and the buffer. At low fields < 500

Oe, the contribution from Cr_2O_3 bulk χH is negligible. The features of low-field $M-T$ in Fig. 3 are from the change in Co's magnetization direction at $T_N = 300$ K as described in Eq. 3. At higher fields, Co's magnetization is saturated in the out-of-plane direction, and the $M-T$ features will be from the bulk χH of Cr_2O_3. The shape of high-field $M-T$ in Fig. 3 is the same as the susceptibility parallel to [0001] growth direction of Cr_2O_3, and the cusp at 300 K corresponds to T_N[41]. The Néel temperature determined from both methods agreed. Thus, the low-field M-T measurement provides an easy method to imply T_N when direct detection is difficult in ultra-thin films of Cr_2O_3. In the next section, we used M-T measurements to study the shift of T_N in ultra-thin films.

The change of magnetization amplitude in the low-field $M-T$ curves is larger for H = 200 Oe compared to 50 Oe (Fig. 3). The reason is not directly visible from Eq. 3. The interface anisotropy J_i can be decomposed into two parts $J_i = J_{i0} + \delta J_i(T)$, where J_{i0} is the larger part resulting from the interface anisotropy of Co with Ru and Pt and it is weakly dependent on temperature, and $\delta J_i(T)$ is small but with a large temperature dependence, and it corresponds to a perpendicular anisotropy due to exchange coupling with Cr_2O_3. Assuming that $\delta J_i(T) \ll J_{i0}$, then Eq. 3 can be approximated to:

$$\begin{aligned}\Delta m_z(T) &= m_z(T) - m_z(T > T_N) \\ &\approx \frac{1}{2}\left(\frac{J_K(T)}{2\pi M_s^2 t_{\mathrm{Co}} - J_{i0}} + \frac{\delta J_i(T) H M_s t_{\mathrm{Co}}}{(2\pi M_s^2 t_{\mathrm{Co}} - J_{i0})^2}\right). \end{aligned} \quad (4)$$

Hence, the presence of a weak perpendicular exchange anisotropy results in a larger Δm_z for a larger H.

As an additional consideration, it is possible to ignore the effects of the exchange-coupling field on shifting T_N. The exchange-coupling field can have the same effects on AFM ordering as an applied magnetic field. It was reported that T_N decreases with an external magnetic field[42]. However, the decrease is negligible on an order of 5–6 mK/kOe by application of a high magnetic field up to 90 kOe. Contrarily, in the case of a strong exchange coupling with Co without a spacer layer, the ordering of Cr_2O_3 interface layer was reported above T_N[43]. In the present report, the exchange coupling is weak through the Ru spacer for $t_{\mathrm{Ru}} > 1.0$ nm. If there is an effect from this weak exchange coupling with Co on T_N, then T_N will be significantly dependent on t_{Ru}. No such a dependence was found.

IV. FINITE-SIZE SCALING AND CORRELATATION LENGTH

Finite-size scaling effects start to be observed when one of the system's dimensions becomes comparable to the characteristic length scale, which is the spin-spin correlation length[44,45]. This is mostly pronounced for thin films, nano-wires, and nano-particles. The variation of T_N with thickness is expected to follow the finite-size scaling relation of[28,44,46,47]:

$$\Delta T_N(t) = \frac{T_N^{\infty} - T_N(t)}{T_N^{\infty}} = \left(\frac{t}{\xi_0}\right)^{-\lambda}, \tag{5}$$

where ΔT_N is the normalized shift in T_N, T_N^{∞} is the Néel temperature in the bulk, $T_N(t)$ is the shifted Néel temperature of the film with a finite thickness t, ξ_0 is the spin-spin correlation length at zero temperature, and λ is the shift exponent related to the critical exponent ($\nu = 1/\lambda$) governing the temperature dependence of the correlation length:

$$\xi(T) = \xi_0 |1 - T/T_N|^{-\nu}. \tag{6}$$

Bulk T_N of Cr_2O_3 can be decreased (increased) by expanding (shrinking) the in-plane lattice spacing as predicted theoretically[23], and subsequently confirmed experimentally[24]. However, a study on the effect of changing bulk T_N on spin-spin correlation in ultra-thin chromia is still lacking.

To study the effects of FSS on T_N of Cr_2O_3, t_{Cr2O3} was varied from 20 nm down to 1 nm. Figure 4(a) shows M-T curves measured at a low out-of-plane field of 50 Oe of samples with a Fe_2O_3 buffer. A decrease of T_N with decreasing t_{Cr2O3} is found. AFM ordering was still present down to t_{Cr2O3} = 1 nm, with T_N = 195 K. By changing the buffer layer to other buffers, different T_N^{∞} were found due to the change in Cr_2O_3 lattice constant (table I). However, the reduction of T_N with reducing t_{Cr2O3} was similar between buffers (Fig. 4(b)). Because the change in T_N normalized by T_N^{∞} did not show a significant dependence on the buffer choice, all of the experimental data of the different buffers were fitted by a single fitting to Eq. 5 on a log-log scale (Fig. 4(c)). The estimated values of ξ_0 and λ were 0.57(6) nm and 1.34(7), respectively (table I).

To confirm that T_N shift is due to the FSS and hence the order estimation of ξ_0 and λ, we simulated the temperature dependence at the magnetic transition using VAMPIRE atomistic simulation package, which is based on Monte-Carlo Metropolis algorithm solution to a classical Heisenberg's spin-Hamiltonian[39]. The Hamiltonian $\mathcal{H}$ is defined as follows:

$$\mathcal{H} = -\sum_{i \neq j} J_{ij} \mathbf{S}_i \cdot \mathbf{S}_j - K_u \sum_i \left(\mathbf{S}_i \cdot \mathbf{c}\right)^2, \tag{7}$$

where J_{ij} is the exchange interaction energy between the normalized spin vectors $\mathbf{S}_i$ and $\mathbf{S}_j$, which reside at the atomic positions i and j. A uniaxial crystalline anisotropy K_u of 2×10^{-5} erg/cc represents the Cr_2O_3 anisotropy along the $\mathbf{c}$-axis[48]. The exchange-interaction energies of the first- and second-nearest neighbors (J_1, J_2) are the most relevant for T_N determination[12,23,49], and they were set to 56.4 and 25.6 meV, respectively. Both of J_1 and J_2 are due to the direct exchange interaction between Cr ions, where J_1 is with a single neighbor in the c-axis direction, and J_2 is with other three ions in the buckled Cr ions plane. A corundum-type lattice structure was simulated, where the lattice parameters were set as $a = 4.951$ Å, and $c = 13.566$ Å[50]. The Cr spin magnetic moment was set to 2.48 Bohr magnetons[51].

The characteristic spin-correlation length ξ_0 was determined by two simulation methods. In simulation 1, we directly calculated the temperature dependence of spin-correlation length and fitted it to Eq. 6. The simulation geometry was a $5 \times 5 \times 5$-nm^3 cube of 5520 Cr spins. At each temperature, 2×10^5 MC steps were used for equilibration, and 5×10^5 steps for time averaging. Then the correlation function Γ between the center spin $\mathbf{S}(\mathbf{0})$ and all other spins $\mathbf{S}(\mathbf{r})$ was calculated from the recorded step-snapshots $\Gamma(\mathbf{r}) = \langle \mathbf{S}(\mathbf{r}) \cdot \mathbf{S}(\mathbf{0}) \rangle$. The result was then fitted to $\Gamma = r^{2-d-\eta} e^{-r/\xi}$, where $d = 3$ is the dimensionality, and η determines the long-range correlation near to T_N. The numerical value of η is not varying considerably among 3-d models with different degrees of freedom[7], and a value of 0.036 was chosen. To confirm that there are no edge effects, two cases were tested with either free or periodic boundary conditions (Fig. 5(b)), and no difference was found. Also, increasing averaging steps to 8×10^5 did not change results. The fitting of temperature dependence of ξ gave the values of ξ_0 and ν at 0.20(2) nm and 0.73(1), respectively (Fig. 5(b)). It needs to be pointed that even though Cr_2O_3 should be anisotropic in ξ_0, we found that ξ_0 is almost equal along the directions parallel and perpendicular to c-axis. The reason is likely that J_1 connect only a single neighbor and J_2 connects three neighbors, making total coupling energies similar in the parallel and perpendicular directions. Therefore, we treated ξ_0 as an isotropic value.

In simulation 2, we calculated T_N variation with thickness in a $15 \times 15 \times t_{\mathrm{Cr2O3}}$-nm^3 simulation geometry ($t_{\mathrm{Cr2O3}} \times 10^4$ spins). To emulate the extended films, boundary conditions

were free in the thickness direction and periodic in the in-plane directions. Temperature was varied from 0 to 350 K in 5-K intervals, and averaging was taken over 2×10^5 MC steps, after 10^5 steps for equilibration. Average sublattice magnetization $\langle M_{sub} \rangle$ was same for both of spin-sublattices. For $t_{\mathrm{Cr2O3}} \leq 1.5$ nm, doubling the total MC steps and reducing the temperature intervals to 3 K did not affect the results. Néel temperature was found from a fitting of temperature dependence of $\langle M_{sub} \rangle$ to $(1 - T/T_N)^{\beta}$, where β is magnetization's critical exponent. A shift of $T_N(t)$ with decreasing thickness is observed (Fig. 5(c)). Notably, the AFM ordering was maintained down to 1 nm, which is smaller than the unit cell of Cr_2O_3. This is due to the correlation length being smaller that the unit cell. Also, each sublattice is connected with other three neighbors along ab-plane. If one of the sublattices along c-axis is missing, the AFM order can be maintained by exchange coupling along ab-plane. Even below 1 nm, the buckled monolayer of a 0.226-nm thickness also maintained AFM order with $T_N = 125$ K, but it was ignored from subsequent discussion due to absence of J_1 coupling. The data points of $T_N(t)$ with the corresponding fitting to Eq. 5 are shown in figures 4(b,c). The bulk T_N of 306 K in units of J_1/k_B is 0.468, where k_B is the Boltzmann constant, which is in agreement with previous reports[12]. The fitted values of ξ_0, λ, and ν are 0.24(2) nm, 1.26(1), and 0.79(1), respectively (Fig. 4(c)). There is a quantitative agreement between the two calculation methods. Also, the critical exponent ν is close to what is expected from the 3-d Ising, XY or Heisenberg universality models having ν in the range of 0.63–0.71[7,9].

Noting the different lattice spacings and exchange-coupling energies, there are quantitative agreements within an order of magnitude in ξ_0 estimations between MC calculations and experiments (Fig. 4(c)). The difference in ξ_0 can be attributed to the simplifications assumed about the coupling energies in the MC calculations. Namely, the far-ranged exchange-coupling of third- to fifth-nearest neighbors and the strain field should increase ξ_0. Both of the experimental and simulation values of the shift exponent λ values agree reasonably with 3-d universality models. So we can conclude that the observed reduction in transition temperature is due to the FSS.

Concerning the effect of surface roughness on the extraction of FSS parameters, the Cr_2O_3 layer can be considered as composed of smaller areas with slowly-varying thicknesses. The local thickness distribution can be represented by Eq. 1. The exchange-coupling energy between Co and Cr_2O_3 layers is weaker than the exchange stiffness of Co. Therefore, the response of Co's magnetization is the average of AFM ordering in Cr_2O_3, and the measured

T_N is the average of the whole Cr_2O_3 layer. The average normalized shift of T_N ($\langle \Delta T_N \rangle$) can be found as follows:

$$\begin{aligned} \langle \Delta T_N \rangle &= \int_0^\infty \Delta T_N P_T dt \\ &= \left(\frac{\langle t_{\mathrm{Cr2O3}} \rangle}{\xi_0} \right)^{-\lambda} \exp\left(\frac{1}{2} s^2 (\lambda + 1) \right), \end{aligned} \tag{8}$$

where $\langle t_{\mathrm{Cr2O3}} \rangle = \exp(\ln t_n + s^2/2)$ is the average thickness. As a first-order approximation for small s^2, the deviation caused by using an average global thickness and neglecting roughness is on order of $s^2/2(\lambda+1)$. This results in <5% error for $s = 0.2$. Therefore, the FSS relation is relatively insensitive to size distribution, as it was shown in Ref.[31]. However, we did not take into account the effects of magnetically-dead interfacial layers and interdiffusion. We assumed them to be minimal in the present study, but such an assumption is not always safe, as shown by Ref.[52].

The spin-correlation length of 0.2–0.6 in Cr_2O_3 is much shorter than what was reported for CoO and NiO of 1.0–2.1 nm and 1.4 nm, respectively[5,28,30,31]. We attribute this difference to the difference in the coordination number of exchange interactions. In the following discussion, the interaction coordination number without regard to non-magnetic ions is considered. Also, we define the nearest-neighbor degree nNN as the number of intermediate magnetic ions that relay the exchange coupling, so that the first-nearest-neighbors 1NN are the spins with direct coupling regardless of being either of superexchange or direct-exchange type. In that sense, in the Cr_2O_3 structure, both J_1 and J_2 are connecting 1NN's. In a simplistic model, the number of paths between far neighbors ($\geq$ 2NN) in a corundum-type Cr_2O_3 crystal are limited to one, *e.g.* spins numbered 1 and 2 in Fig. 6(a). On the other hand, in the rock-salt structure with only 1NN interactions, there are at least 4 paths of coupling between 2NN's, which are marked as 1 and 2 in Fig. 6(b). Also, the number of paths does not decay rapidly with distance. This can explain qualitatively the difference between correlation lengths in close-packed crystals and corundum-type.

In the discussion above, we only considered Cr_2O_3 with J_1 and J_2 interactions. Adding more far-ranged exchange interactions can increase the correlation length. Kota *et al.* reported a doubling of correlation length in Cr_2O_3 at the interface with an Fe_2O_3 layer[37]. This is due to additional superexchange-type interactions with a longer range at the oxygen-divided interface. However, we did not find an effect of Fe_2O_3 or Ir-Fe_2O_3 buffer layers on

the relative T_N shift of Cr_2O_3 (Fig. 4(c)). In order to minimize the surface charge, the corundum-type crystals prefer to terminate in the bottom layer of the buckled metal layer (ion No. 2 in Fig. 6(a))[53]. Therefore, it is likely that the interface of Fe_2O_3/Cr_2O_3 is a metal-split one, which is not different from a stand-alone Cr_2O_3 crystal[37]. If an oxygen-divided interface can be realized, the correlation length can be increased by the effect of Fe_2O_3 buffer layer.

V. CONCLUSION

We presented a study on the effect of finite-size scaling on the antiferromagnetic order of corundum-type Cr_2O_3 ultra-thin films. The films were epitaxially grown by reactive sputtering, and were 1–20 nm in thickness. The Néel temperature T_N was determined by a relatively-easy method of measuring the effect of an optimized exchange-coupling on a proximate ferromagnetic layer. By controlling the lattice spacings of Cr_2O_3 films, different bulk Néel temperature values T_N^∞ could be achieved on different buffer layers. For each buffer layer, T_N monotonically decreased when the film thickness was decreased, in accordance with finite-size scaling. The spin-correlation length ξ_0 and the shift exponent λ obtained from the experimental results did not show a significant dependence on T_N^∞ and the choice of buffer layer. Monte-Carlo simulations of the spin-spin correlation function and the finite-size effects also agreed reasonably with the experimental results. Moreover, the shift exponents λ were close with the expectations from three-dimensional universalities. We found that ξ_0 of Cr_2O_3 was much smaller than what was reported for CoO, NiO, and other close-packed crystals. We attribute this change to the difference between corundum-type and rock-salt-type crystals in the number of exchange-coupling paths between far neighbors. The understanding the critical behavior of ultra-thin Cr_2O_3 films should pave the way for more work on realizing ultra-thin magnetoelectric storage media having a high Néel temperature.

ACKNOWLEDGMENTS

The authors thank Dr. Richard Evans for his comments and the VAMPIRE community for their support. This work was partly funded by ImPACT Program of Council for Science, Technology and Innovation (Cabinet Office, Japan Government).

* sppati@ecei.tohoku.ac.jp

† mahdawi@ecei.tohoku.ac.jp

[1] M. S. Green and J. L. Lebowitz, *Phase transitions and critical phenomena*, Vol. 8 (Academic Press, 1983).

[2] R. Merservey and B. B. Schwartz, in *Superconductivity*, Vol. 1, edited by R. D. Parks (Marcel Dekker, Inc., 1969) p. 117.

[3] B. Y. Jin and J. B. Ketterson, Advances in Physics **38**, 189 (1989).

[4] D. McCauley, R. E. Newnham, and C. A. Randall, Journal of the American Ceramic Society **81**, 979 (1998).

[5] X. Y. Lang, W. T. Zheng, and Q. Jiang, Physical Review B **73**, 224444 (2006)and references therein.

[6] D. S. Ritchie and M. E. Fisher, Physical Review B **5**, 2668 (1972).

[7] J. C. Le Guillou and J. Zinn-Justin, Physical Review B **21**, 3976 (1980) and references therein.

[8] J. C. Le Guillou and J. Zinn-Justin, Journal de Physique Lettres **46**, 5 (1985).

[9] M. Ferer and A. Hamid-Aidinejad, Physical Review B **34**, 6481 (1986).

[10] K. Chen, A. M. Ferrenberg, and D. P. Landau, Physical Review B **48**, 3249 (1993).

[11] X. He, W. Echtenkamp, and C. Binek, Ferroelectrics **426**, 81 (2012).

[12] A. K. Murtazaev, Low Temperature Physics **25**, 344 (1999); A. K. Murtazaev, I. K. Kamilov, and K. K. Aliev, Journal of Magnetism and Magnetic Materials **204**, 151 (1999).

[13] Y. Kota, H. Imamura, and M. Sasaki, Journal of Applied Physics **115**, 17D719 (2014).

[14] P. Borisov, A. Hochstrat, X. Chen, W. Kleemann, and C. Binek, Physical Review Letters **94**, 117203 (2005).

[15] X. He, Y. Wang, N. Wu, A. N. Caruso, E. Vescovo, K. D. Belashchenko, P. A. Dowben, and C. Binek, Nature Materials **9**, 579 (2010).

[16] T. Ashida, M. Oida, N. Shimomura, T. Nozaki, T. Shibata, and M. Sahashi, Applied Physics Letters **104**, 152409 (2014).

[17] T. Ashida, M. Oida, N. Shimomura, T. Nozaki, T. Shibata, and M. Sahashi, Applied Physics Letters **106**, 132407 (2015).

[18] K. Toyoki, Y. Shiratsuchi, A. Kobane, S. Harimoto, S. Onoue, H. Nomura, and R. Nakatani, Journal of Applied Physics **117**, 17D902 (2015).

[19] K. Toyoki, Y. Shiratsuchi, A. Kobane, C. Mitsumata, Y. Kotani, T. Nakamura, and R. Nakatani, Applied Physics Letters **106**, 162404 (2015).

[20] K. D. Belashchenko, O. Tchernyshyov, A. A. Kovalev, and O. A. Tretiakov, Applied Physics Letters **108**, 132403 (2016).

[21] M. Matsuzaki, K. Shinohara, T. Shibata, M. Sahashi, and T. Nozaki, "Magnetic recording system and magnetic recording device," U.S. Patent No. 8,724,434 (2014).

[22] T. Shibata and M. Sahashi, "Magnetization controlling element using magnetoelectric effect," U.S. Patent App. 14/532,533 (2015).

[23] Y. Kota, H. Imamura, and M. Sasaki, Applied Physics Express **6**, 113007 (2013).

[24] S. P. Pati, N. Shimomura, T. Nozaki, T. Shibata, and M. Sahashi, Journal of Applied Physics **117**, 17D137 (2015).

[25] S. Mu, A. Wysocki, and K. Belashchenko, Physical Review B **87**, 054435 (2013).

[26] M. Street, W. Echtenkamp, T. Komesu, S. Cao, P. A. Dowben, and C. Binek, Applied Physics Letters **104**, 222402 (2014).

[27] M. J. Carey and A. E. Berkowitz, Journal of Applied Physics **73**, 6892 (1993).

[28] T. Ambrose and C. L. Chien, Physical Review Letters **76**, 1743 (1996).

[29] P. J. van der Zaag, Y. Ijiri, J. A. Borchers, L. F. Feiner, R. M. Wolf, J. M. Gaines, R. W. Erwin, and M. A. Verheijen, Physical Review Letters **84**, 6102 (2000).

[30] E. N. Abarra, K. Takano, F. Hellman, and A. E. Berkowitz, Physical Review Letters **77**, 3451 (1996).

[31] M. Molina-Ruiz, A. F. Lopeandía, F. Pi, D. Givord, O. Bourgeois, and J. Rodríguez-Viejo, Physical Review B **83**, 140407 (2011).

[32] S. Park, H. Jang, J.-Y. Kim, B.-G. Park, T.-Y. Koo, and J.-H. Park, EPL (Europhysics Letters) **103**, 27007 (2013).

[33] L. Frangou, S. Oyarzn, S. Auffret, L. Vila, S. Gambarelli, and V. Baltz, Physical Review Letters **116**, 077203 (2016).

[34] S. Chambers, Y. Liang, and Y. Gao, Physical Review B **61**, 13223 (2000).

[35] N. Shimomura, S. P. Pati, Y. Sato, T. Nozaki, T. Shibata, K. Mibu, and M. Sahashi, Journal of Applied Physics **117**, 17C736 (2015).

[36] T. Mitsui, K. Mibu, M. Seto, M. Kurokuzu, S. P. Pati, T. Nozaki, and M. Sahashi, Journal of the Physical Society of Japan **85**, 063601 (2016).

[37] Y. Kota, H. Imamura, and M. Sasaki, IEEE Transactions on Magnetics **50**, 1 (2014).

[38] N. Shimomura, S. P. Pati, T. Nozaki, T. Shibata, and M. Sahashi, arXiv:1605.03680 [cond-mat] (2016).

[39] R. F. L. Evans, W. J. Fan, P. Chureemart, T. A. Ostler, M. O. A. Ellis, and R. W. Chantrell, Journal of Physics: Condensed Matter **26**, 103202 (2014).

[40] K. D. Belashchenko, Physical Review Letters **105**, 147204 (2010).

[41] T. R. McGuire, E. J. Scott, and F. H. Grannis, Physical Review **102**, 1000 (1956).

[42] A. Iyama and T. Kimura, Physical Review B **87**, 180408 (2013).

[43] Y. Shiratsuchi, Y. Kotani, S. Yoshida, Y. Yoshikawa, K. Toyoki, A. Kobane, R. Nakatani, and T. Nakamura, AIMS Materials Science **2**, 484 (2015).

[44] M. Barber, in *Phase transitions and critical phenomena*, Vol. 8, edited by M. S. Green and J. L. Lebowitz (Academic Press, 1983) pp. 145–266.

[45] V. Privman, *Finite Size Scaling and Numerical Simulation of Statistical Systems* (WORLD SCIENTIFIC, 1990).

[46] M. E. Fisher and M. N. Barber, Physical Review Letters **28**, 1516 (1972).

[47] K. Binder and P. C. Hohenberg, Physical Review B **9**, 2194 (1974).

[48] S. Foner, Physical Review **130**, 183 (1963).

[49] E. J. Samuelsen, M. T. Hutchings, and G. Shirane, Physica **48**, 13 (1970).

[50] L. W. Finger and R. M. Hazen, Journal of Applied Physics **51**, 5362 (1980).

[51] P. J. Brown, J. B. Forsyth, E. Lelièvre-Berna, and F. Tasset, Journal of Physics: Condensed Matter **14**, 1957 (2002).

[52] Y. J. Tang, D. J. Smith, B. L. Zink, F. Hellman, and A. E. Berkowitz, Physical Review B **67**, 054408 (2003).

[53] X.-G. Wang, A. Chaka, and M. Scheffler, Physical Review Letters **84**, 3650 (2000).

Figure 1. The height distribution of a 1.5-nm Cr_2O_3 surface grown over an Ir-Fe_2O_3 buffer. The fitting (red line) to a log-normal distribution gives a shape parameter s of 0.036. The inset shows the corresponding topography scan.

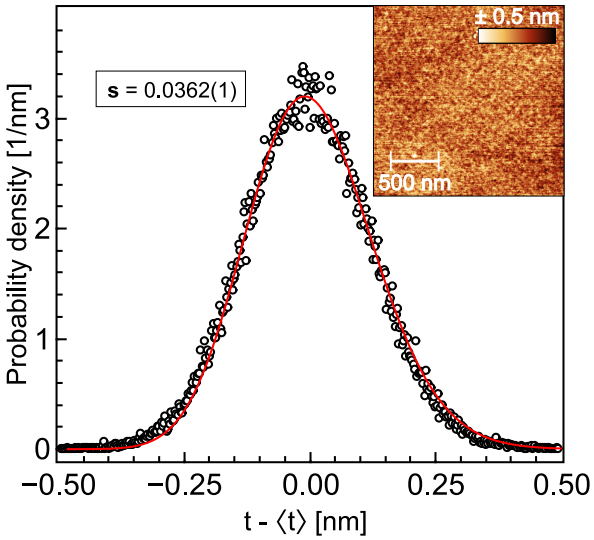

Figure 2. (a) A schematic of T_N detection method. The anisotropy of Co layer is optimized such that the ordering of Cr_2O_3 spins changes the tilting of Co magnetization from inplane above T_N to an out-of-plane direction below T_N. A Ru metallic spacer layer is used to tune the exchange coupling energy J_K and interfacial perpendicular anisotropy. The definitions of magnetic field H and magnetization equilibration angle θ_0 are indicated. (b) Dependence of the total exchange coupling energy J_K on Ru spacer thickness t_{Ru} found from magnetization hysteresis loops at 100 K. J_K monotonically decreases against the thickness of Ru. (c) Dependence of low-field magnetization normalized to saturation magnetization M_r/M_s on t_{Ru}. At $1.25 \leq t_{\mathrm{Ru}} \leq 1.5$ nm, a large change in M_r/M_s is found above and below T_N. (d) The change of M-H loops with changing t_{Ru} is shown. For thin Ru ($t_{\mathrm{Ru}} \leq 1.0$), a dominant perpendicular anisotropy remains above and below T_N. At an intermediate thickness of 1.25–1.50 nm, there is a large change of magnetization's easy direction upon crossing T_N. In (b),(c), and (d) a 25-nm Pt buffer was used and the solid-lines are eye-guides.

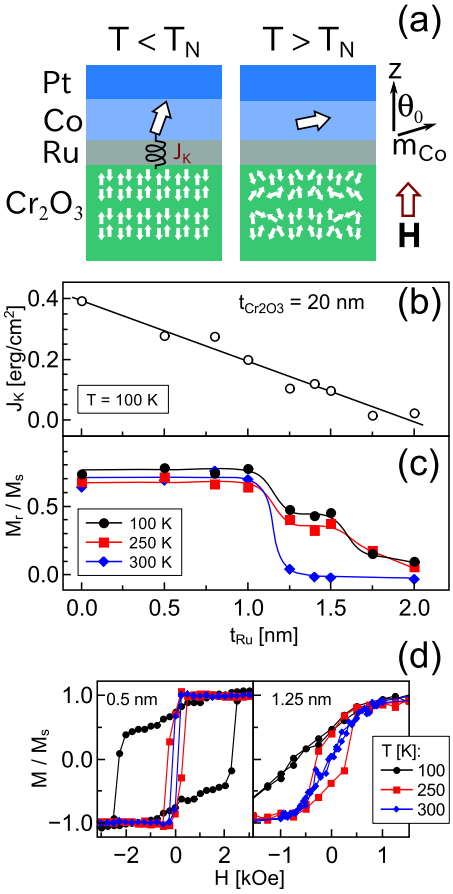

Figure 3. Comparison between low-field and high-field M-T curves of Pt (25)/ Cr_2O_3 (1000)/Ru (1.25)/Co (1)/Pt (5). To remove the contribution of the substrate's diamagnetic response, the change in the total magnetization with respect to T_N is plotted against temperature. The low-field M-T curves correspond to the change in Co magnetization direction, and to the Cr_2O_3 susceptibility response χH-T at high fields. Both measurements agree on a T_N of ≈300 K.

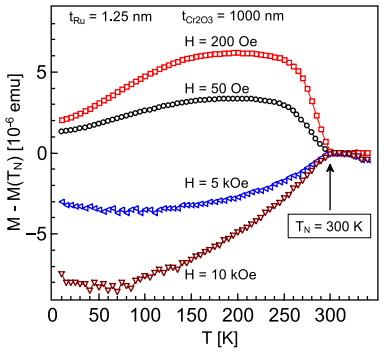

Figure 4. (a) M-T curves under $H = 50$ Oe for Fe_2O_3-buffered Cr_2O_3 (t_{Cr2O3})/Ru (1.25)/Co (1)/Pt (5), where $t_{Cr2O3} = 20$, 10, 5, 3, and 1 nm. (b) The shift of T_N with t_{Cr2O3} is shown for different buffers, in addition to Monte-Carlo simulations. (c) A log-log plot of normalized T_N versus t_{Cr2O3}. Solid lines are fittings to Eq. 5. The characteristic spin-correlation length ξ_0 is indicated by an extrapolation to the vanishing point of T_N. Shift exponent λ is determined from the slope. Both ξ_0 and λ are in a reasonable agreement among experiments and simulation.

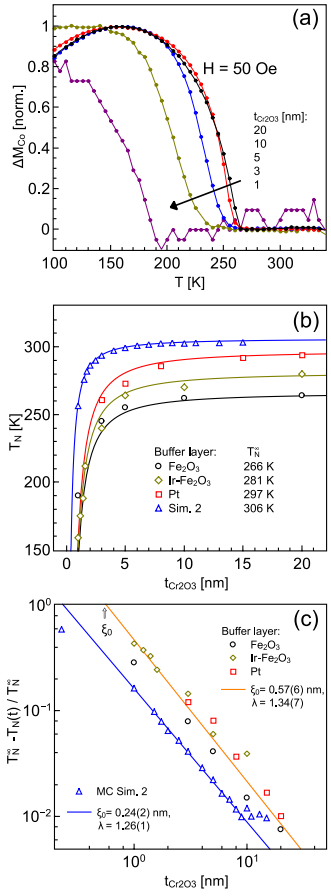

Figure 5. Monte-Carlo (MC) simulation results of spin-correlation length using (a,b) simulation method 1, and (c) simulation method 2. (a) A direct calculation of correlation function Γ between center spin $\mathbf{S}(\mathbf{0})$ and all other spins $\mathbf{S}(\mathbf{r})$ in a $5 \times 5 \times 5$-nm^3 geometry. The temperature-dependent correlation length ξ is found from a fitting to $\Gamma = r^{-1.036} e^{-r/\xi}$. (b) Temperature dependence of ξ in the cases of including or disabling periodic boundary conditions. Both cases produce the same results. Inset is a log-log plot with a linear fitting to the power law in Eq. 6. (c) Thickness dependence of T_N determined from the sublattice magnetization $\langle M_{\rm sub} \rangle$. The finite thickness results in a decrease in T_N when it approaches spin-correlation length. T_N values are summarized in Fig. 4(b) and (c). The estimations of ξ_0 and λ from both simulation methods are in a reasonable agreement [Figs. 4(c) and 5(b)].

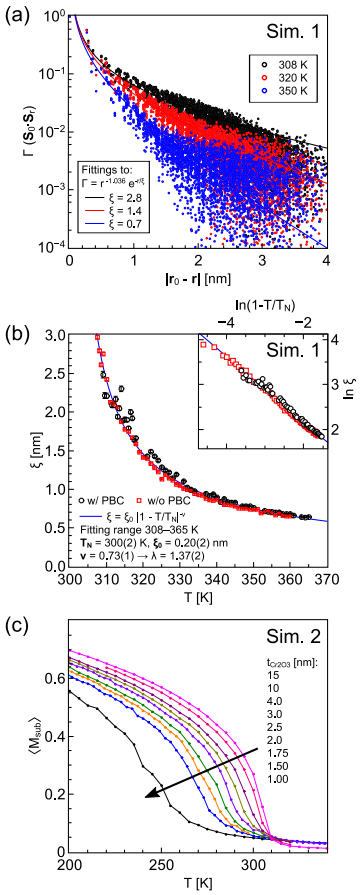

Figure 6. Plane projections of (a) corundum and (b) rock-salt crystal structures on $(11\bar{2}0)$ and (100) planes, respectively. Differences in the coordination number of exchange interactions result in a different correlation length for each crystal system. It can be seen by counting the number of indirect connections between far neighbors, *e.g.* spins marked by numbers 1 and 2. The rock-salt structure has more connections in comparison to corundum-type structure.